PHYSICAL REVIEW C VOLUME 21, NUMBER 5 MAY 1980

Systematic features of the pion-nucleus interaction

R. S. Bhalerao, L. C. Liu, and C. M. Shakin
Department of Physics and Institute for Nuclear Theory, Brooklyn College of the City University of New York, Brooklyn, New York 11210
(Received 20 June 1979)

We analyze pion elastic-scattering data for ^{40}Ca and ^{48}Ca using a covariant theory of the optical potential developed previously. Combining these results with the information obtained from the analysis of pion scattering from ^{12}C and ^{16}O reported earlier, we are able to discuss the systematics of the pion-nucleus optical potential. Our model contains a first-order optical potential which is obtained from a parameter-free calculation. The parameters of a second-order potential are determined by requiring that the sum of the first- and second-order potentials provides a fit to the elastic-scattering data. The parameters of the second-order potential exhibit a smooth dependence on energy and target mass number. These parameters have a marked resonance behavior. We find that the maximum value of the magnitude of the imaginary part of the second-order potential occurs at about 150 MeV while the first-order potential has a maximum for the magnitude of the imaginary part at about 240 MeV. The imaginary part of the first-order potential has a width at half maximum of about 200 MeV. This corresponds to a *kinematic* broadening of the (3,3) resonance due to the effects of the Fermi motion of the target nucleons. (This increased width is unrelated to the effects of the true absorption process or of collision broadening.) We also find a significant isospin violation in the second-order potential. For example, the imaginary part of the second-order potential for π^- scattering is found to be systematically larger than that for π^+ scattering for nuclei with $N = Z$. An explanation for this feature of the optical potential is presented.

[NUCLEAR REACTIONS Elastic scattering of pions from ^{40}Ca (40–241 MeV) and ^{48}Ca (130 MeV). Systematics of first- and second-order optical potentials.]

I. INTRODUCTION

Pion elastic-scattering data for some light nuclei (^{4}He, ^{12}C, and ^{16}O) were analyzed successfully[1] using a covariant scattering theory.[2] In these calculations a complete integration over the Fermi motion of the target nucleons was carried out and the off-shell effects related to nuclear binding were treated carefully.[3] The first-order optical potential is parameter-free and is believed to be quite accurate. Parameters of the second-order phenomenological potential were determined by fitting the experimentally determined differential cross sections for elastic scattering. In general, the parameters for ^{12}C and ^{16}O varied smoothly with pion energy and exhibited a marked resonance behavior.[1]

In the present work we have tested the validity of the aforementioned parametrization in the medium-mass region. In particular, we have studied the importance of the first- and second-order optical potentials for pion scattering on ^{40}Ca and ^{48}Ca at all the energies for which experimental data are available. The systematics of the variation of the optical potential with pion energy and target mass are investigated. With some exceptions, parameters for ^{12}C and ^{16}O were found to be similar in the earlier work.[1] Hence, exploring the possibility of a universal parametrization of the optical potential was one of the motivations of the present work.

The problem of determining the neutron matter distribution in the calcium isotopes has received some attention. Information may be obtained from the conventional methods of α-nucleus[4] or proton-nucleus scattering.[5] Recently measurements of π-nucleus scattering cross sections near the (3, 3) resonance have been made to study the neutron-matter radii in the calcium isotopes.[6] Another aim of our work was to study the utility of pion-nucleus scattering for the determination of neutron-matter radii. We conclude, however, that there does not seem to be much possibility of learning about the neutron-matter distribution from the studies reported here.

We believe that our studies do provide significant insight concerning the interaction of pions with nuclei. In particular, the pion-nucleus optical potential is found to exhibit some extremely interesting systematic features. We believe our analysis should stimulate further microscopic studies of pion-nucleus dynamics.

II. STRUCTURE OF THE SECOND-ORDER POTENTIAL

Pion-nucleus optical potential can be written as

$$\langle \vec{k}' | V_C | \vec{k} \rangle + \langle \vec{k}' | V^{(1)}(W) | \vec{k} \rangle + \langle \vec{k}' | V^{(2)}(W) | \vec{k} \rangle ,$$

where V_C is the Coulomb potential and $V^{(1)}$ and

$V^{(2)}$ are the first- and second-order optical potentials, respectively. The calculation of the first-order potential has been extensively discussed previously.[2] We note that we have used a (spherical) Hartree-Fock code to calculate the neutron and proton wave functions which are required in the calculation of the first-order potential. (The charge density constructed from these wave functions is consistent with electron scattering data.) Experimental separation energies are used for the least bound nucleons.

In the absence of a microscopic calculation of the second-order potential we have introduced a phenomenological model by writing[1,7]

$$\langle \vec{k}' | V^{(2)}(W) | \vec{k} \rangle = R^{1/2}(\vec{k}')2M_A A(A-1)\bar{G}(\vec{k}-\vec{k}') \times [B(W)+C(W)\vec{k}\cdot\vec{k}']R^{1/2}(\vec{k}). \quad (2.1)$$

Here R is a kinematical factor defined as[1]

$$R(\vec{k}) = \frac{E_\pi(\vec{k}_0)+E_A(\vec{k}_0)}{4E_\pi(\vec{k}_0)E_A(\vec{k}_0)} \cdot \frac{1}{E_\pi(\vec{k})+E_A(\vec{k})} \quad (2.2)$$

Further,

$$W = (\vec{k}_0^{\,2}+m_\pi^{\,2})^{1/2} + (\vec{k}_0^{\,2}+M_A^{\,2})^{1/2} \quad (2.3)$$

and

$$\bar{G}(\vec{k}-\vec{k}') = (2\pi)^3 \int \exp[i(\vec{k}-\vec{k}')\cdot\vec{r}]\rho^2(\vec{r})d\vec{r}. \quad (2.4)$$

Here $\vec{k}_0$ is the pion momentum in the π-nucleus center-of-mass frame and $\rho(\vec{r})$ is the nuclear matter density. In Eq. (2.1), B and C are complex parameters to be determined at each energy by performing a χ^2 fit to the experimental differential cross sections. The parameters B and C are determined in what may be termed an energy-

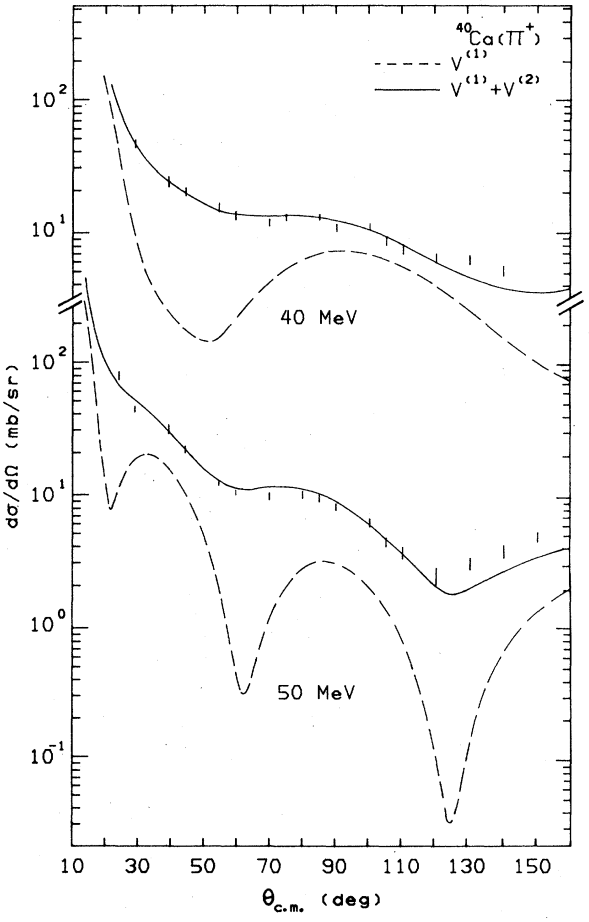

FIG. 1. Differential cross sections for π^+-^{40}Ca elastic scattering at 40 and 50 MeV. The data are taken from Ref. 9. Dashed curve: first-order potential only; solid curve: first- and second-order potentials included.

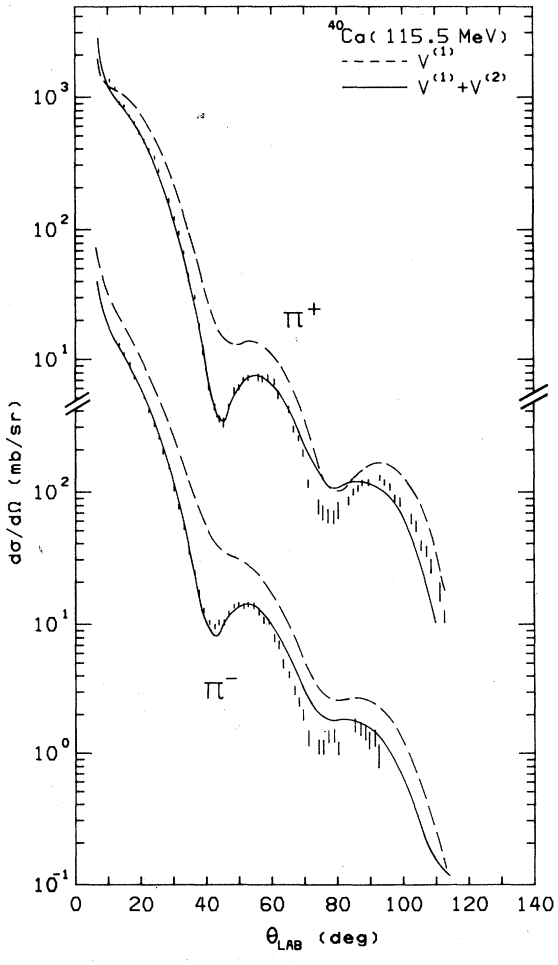

FIG. 2. Differential cross sections for $\pi^\pm$-^{40}Ca elastic scattering at 115.5 MeV. The data are taken from Ref. 8. Dashed and solid curves have the same meaning as in Fig. 1.

dependent manner; that is, no smooth energy dependence of these parameters is assumed before a χ^2 analysis is carried out. We also remark that the data for the total cross sections have not been used in the χ^2-fitting procedure. Details of similar calculations may be found in Ref. 1.

III. RESULTS AND DISCUSSION

Calculated cross sections are presented and compared with the experimental data in Figs. 1–6. The $^{40}Ca(\pi^{\pm})$ data at 115.5, 163.5, and 241 MeV are from Ref. 8. Uncertainty in the absolute normalization of these data is estimated to be $\leq 15\%$.[8] Similarly, the ^{40}Ca (130 MeV) and ^{48}Ca (130 MeV) data[9] have absolute normalization errors of $\pm 5\%$. In Figs. 1–6 the dashed curves represent cross sections calculated with $V^{(1)}$ only and the solid curves represent calculations with $V^{(1)} + V^{(2)}$. (The Coulomb potential is included in all these calculations.)

As can be seen from Figs. 1–6, the second-order optical potential is quite important for the two nuclei studied. This result is consistent with the earlier calculations[1] for lighter nuclei (^{4}He, ^{12}C, and ^{16}O). The relative importance of the second-order potential varies with scattering angle and with pion energy. The former dependence is understandable because of the different radial shapes of the Coulomb, the first-order potential ($\sim\rho$), and the second-order potential ($\sim\rho^2$).

In Figs. 7 and 8 we have presented the real and imaginary parts of k_0^2C, for various pion energies, for the nuclei ^{12}C, ^{16}O, and ^{40}Ca. Table I gives the values of the complex parameters B and k_0^2C. In general, the imaginary part of B is very

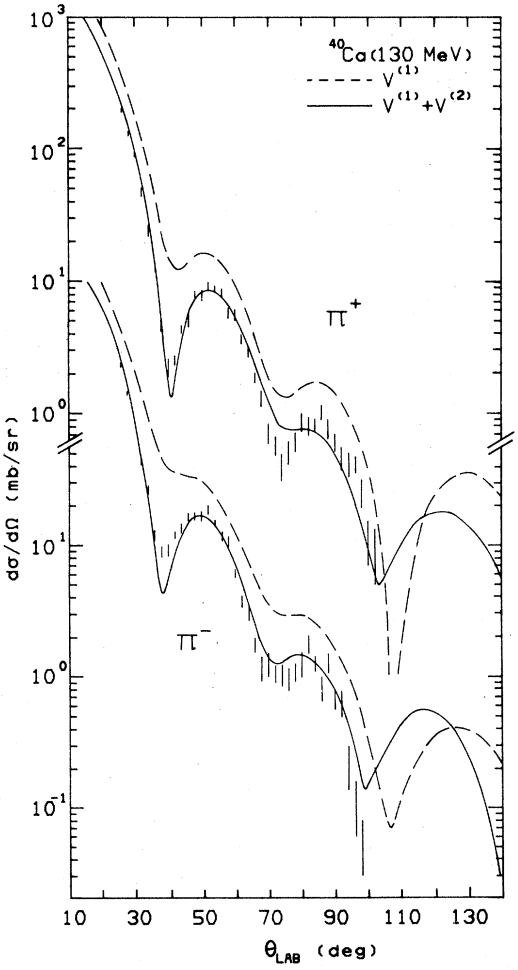

FIG. 3. Same as Fig. 2 with $T_\pi = 130$ MeV, however, the data are taken from Ref. 9.

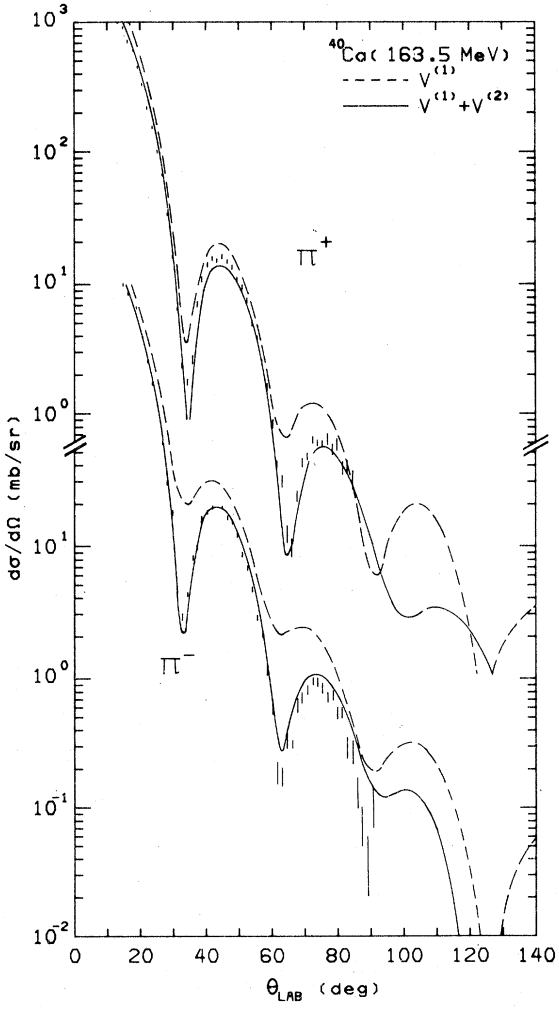

FIG. 4. Same as Fig. 2 with $T_\pi = 163.5$ MeV.

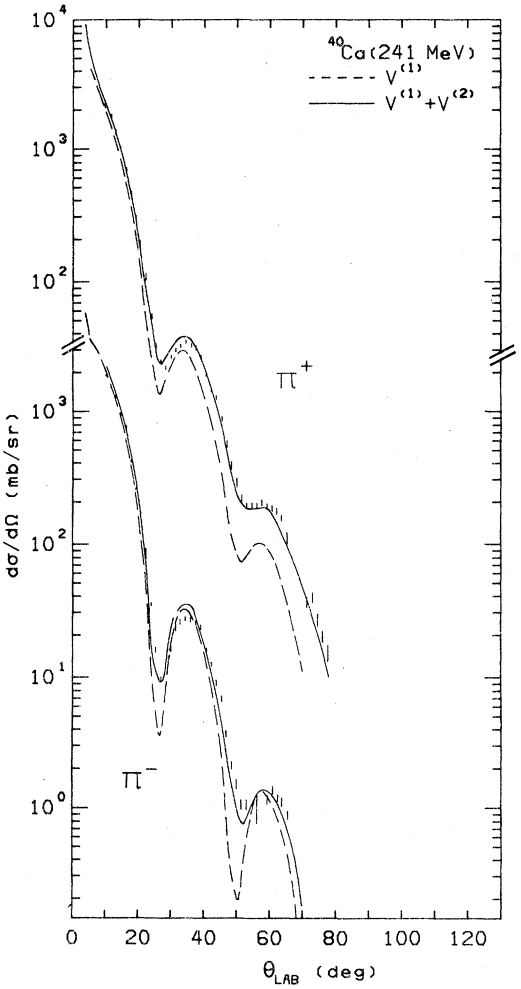

FIG. 5. Same as Fig. 2 with $T_\pi = 241$ MeV.

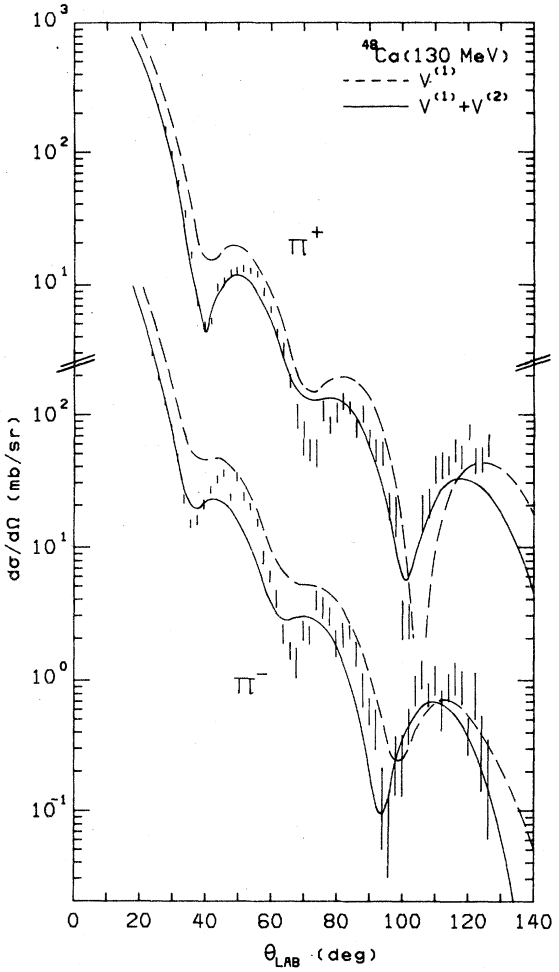

FIG. 6. Differential cross sections for $\pi^{\pm}$-^{48}Ca elastic scattering at 130 MeV. The data are taken from Ref. 9. Dashed and solid curves have the same meaning as in Fig. 1.

small compared to the imaginary part of k_0^2C, hence a graph of $\mathrm{Im}(B)+\mathrm{Im}(k_0^2C)$ would be very similar to that of Fig. 8. Except for the lowest energies, ReB is smaller than Rek_0^2C. The fit for π^- scattering from ^{48}Ca (Fig. 6) is not very good and therefore we believe the numbers given in the last row of Table I are subject to modification. Since we only have data for ^{48}Ca at a single energy (130 MeV) we have not been able to study the systematic behavior of the potential parameters for this nucleus. We believe that more data are required before we can fully understand the optical potential for such nuclei with $N \neq Z$.

Some interesting trends emerge from Figs. 7 and 8. First of all, all the curves show a marked resonance behavior, a feature probably related to the resonance in the true-pion-absorption (TPA) process. [Landau and Thomas have used the knowledge of the cross section for the reaction $\sigma_{\mathrm{tot}}(\pi^+ d \to pp)$ to estimate the magnitude of the potential describing the TPA process.[7] Other authors have performed microscopic calculation of of the absorption process.[10] The description of TPA is also an essential aspect of isobar-hole calculations[11] and gives rise to an important contribution to the Δ isobar self-energy.] In the absence of a fully microscopic calculation for finite nuclei, it is not certain whether processes other than TPA which contribute to $V^{(2)}$ would also exhibit a resonancelike behavior. (See, however, Ref. 1 for a discussion of this point.) Again referring to Figs. 7 and 8 we see that the magnitudes of both Re(k_0^2C) and Im(k_0^2C) generally decrease with increasing nuclear mass. Exceptions to this trend, e.g., the curve for ^{40}Ca(π^-) which lies between the curves for ^{16}O(π^-) and ^{12}C(π^-) in Fig. 8, may be thought of as

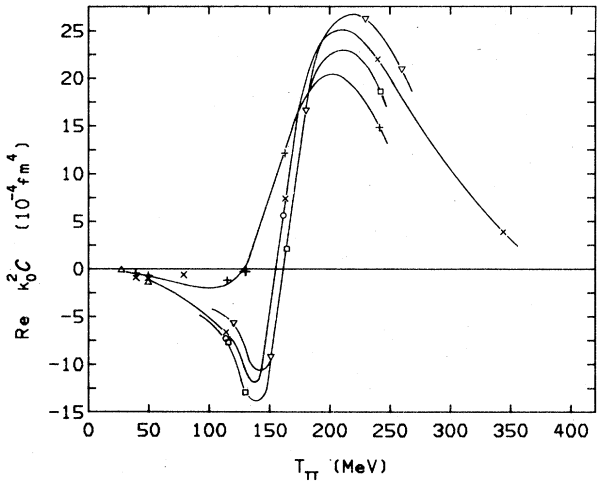

FIG. 7. Re(k_0^2C) as a function of pion kinetic energy for various nuclei. Curves are drawn only as a guide to the eye. Δ: $^{12}C(\pi^+)$, ∇: $^{12}C(\pi^-)$, ×: $^{16}O(\pi^+)$, O: $^{16}O(\pi^-)$, +: $^{40}Ca(\pi^+)$, □: $^{40}Ca(\pi^-)$.

arising due to the "splitting" of a single ^{40}Ca curve into two curves, one corresponding to π^+ and the other to π^- (see below). We note that the positions of the minima in Fig. 8 seem to be shifting toward lower energies as A increases. Similar behavior is observed in Fig. 7 also, where the point at which a curve crosses the axis seems to move to smaller energy as A increases. In Fig. 8 the curves for $^{16}O(\pi^-)$ and $^{40}Ca(\pi^-)$ lie below those for $^{16}O(\pi^+)$ and $^{40}Ca(\pi^+)$, respectively.

It is somewhat more instructive to directly consider the potential $V^{(2)}$ rather than the parameters B and k_0^2C. Therefore we proceed to discuss the matrix elements of the first- and

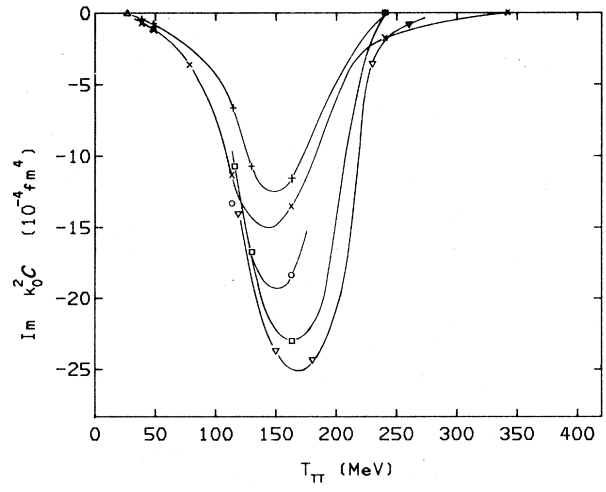

FIG. 8. Same as Fig. 7 for Im(k_0^2C).

TABLE I. Parameters of the second-order potential for $\pi^\pm$ scattering on ^{40}Ca and ^{48}Ca (in units of 10^{-4} fm^4).

	T_π (MeV)	ReB	ImB	Rek_0^2C	Imk_0^2C
^{40}Ca, π^+	40	0.837	−0.294	−0.457	−0.503
^{40}Ca, π^+	50	1.06	−0.280	−0.727	−0.839
^{40}Ca, π^+	115.5	0.571	~0	−1.19	−6.74
^{40}Ca, π^-	115.5	2.36	−0.002	−7.47	−10.7
^{40}Ca, π^+	130	0.766	~0	−0.149	−10.7
^{40}Ca, π^-	130	5.14	−0.007	−12.8	−16.7
^{40}Ca, π^+	163.5	−4.18	−0.012	11.7	−11.7
^{40}Ca, π^-	163.5	2.56	~0	2.15	−22.9
^{40}Ca, π^+	241	1.15	−0.949	14.7	~0
^{40}Ca, π^-	241	−1.88	~0	18.5	~0
^{48}Ca, π^+	130	0.242	−0.530	0.713	−4.11
^{48}Ca, π^-	130	0.559	−0.001	4.00	−0.596

second-order optical potentials. The real and imaginary parts of the (on-shell) matrix elements $\langle\vec{k}|V^{(1)}|\vec{k}\rangle$ and $\langle\vec{k}|V^{(2)}|\vec{k}\rangle$ are shown in Figs. 9–12 for both ^{16}O and ^{40}Ca. It is evident from these figures that both the real and imaginary parts of $\langle\vec{k}|V^{(1)}|\vec{k}\rangle$ and $\langle\vec{k}|V^{(2)}|\vec{k}\rangle$ vary smoothly with energy. This is remarkable since no such energy dependence was presumed before the χ^2 analysis was made. The first-order potential is nearly the same for π^+ and π^-, the small differences arising from differences in the binding energies of the proton and neutron orbits. As might be expected, the matrix elements of $V^{(1)}$ are proportional to the mass number of the target. The value of $|\mathrm{Im}\langle\vec{k}|V^{(1)}|\vec{k}\rangle|$ has a maximum at about 240 MeV and the width at half maximum (Fig. 10) is about 200 MeV for ^{16}O and

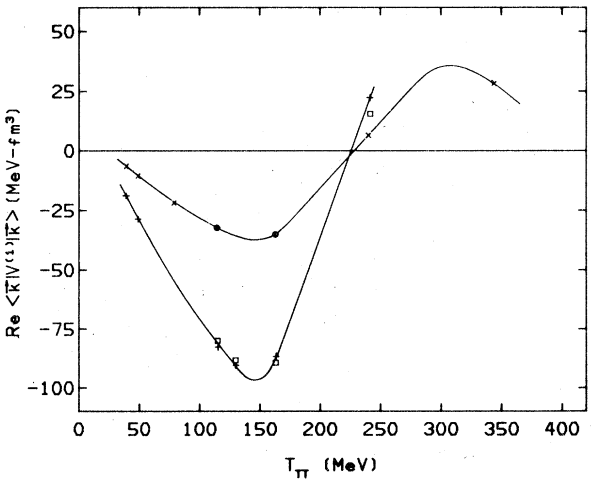

FIG. 9. Real part of $\langle\vec{k}|V^{(1)}|\vec{k}\rangle$ vs pion energy. ×: $^{16}O(\pi^+)$, O: $^{16}O(\pi^-)$, +: $^{40}Ca(\pi^+)$, □: $^{40}Ca(\pi^-)$. Curves are drawn only as a guide to the eye.

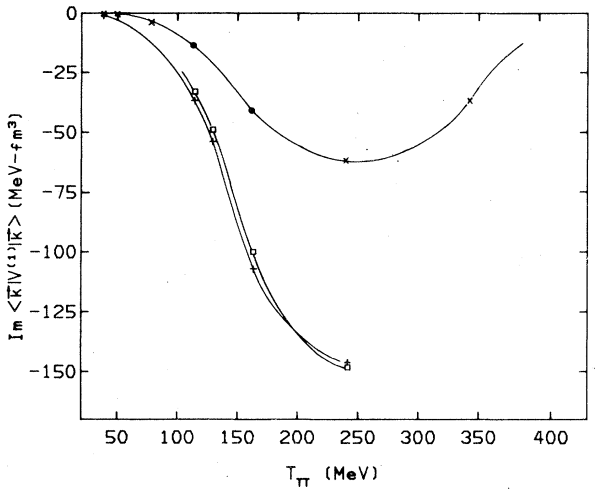

FIG. 10. Same as Fig. 9 for $\mathrm{Im}\langle\vec{k}|V^{(1)}|\vec{k}\rangle$.

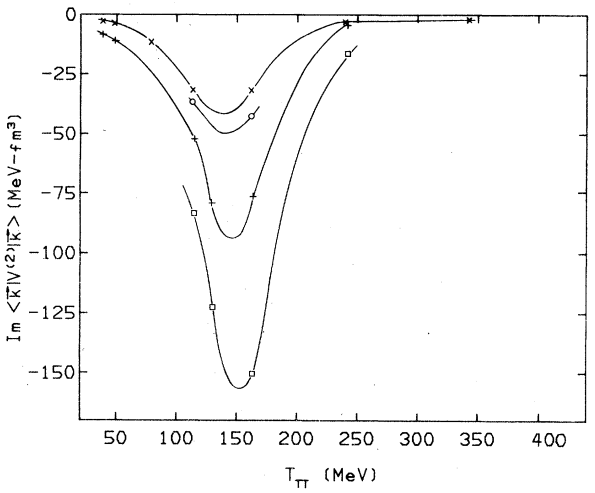

FIG. 12. Same as Fig. 9 for $\mathrm{Im}\langle\vec{k}|V^{(2)}|\vec{k}\rangle$.

^{40}Ca. (See Sec. IV.) The maximum appears at 240 MeV since the effect of Fermi motion of the target nucleons and binding effects cause the π-N T matrix to be evaluated at energies which are significantly below the fixed-scatterer value.[12] This aspect of our calculation of the first-order potential has been discussed previously.[1]

Figures 11 and 12 exhibit the real and imaginary parts of the matrix element $\langle\vec{k}|V^{(2)}|\vec{k}\rangle$. First we note that the maximum value of $|\mathrm{Im}\langle\vec{k}|V^{(2)}|\vec{k}\rangle|$ is at about 140–150 MeV for ^{16}O and ^{40}Ca (see Sec. IV). Most remarkable, however, is the large violation of isospin symmetry exhibited by the second-order potential. We see that the second-order potential is significantly more absorptive for π^- mesons that for π^+ mesons. [Large differences are also to be noted for the real parts of $V^{(2)}$ for π^+ and π^- mesons—see Fig. 11.]

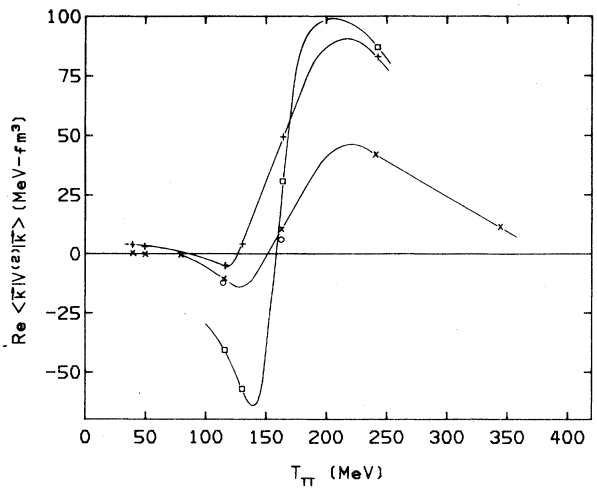

FIG. 11. Same as Fig. 9 for $\mathrm{Re}\langle\vec{k}|V^{(2)}|\vec{k}\rangle$.

To some degree the difference in the values of $V^{(2)}$ for π^- and π^+ mesons provide some further support for the conjecture that $V^{(2)}$ mainly describes the effects of the true pion absorption: We note that in the resonance region the absorption of a π^- meson on a nucleon pair would predominantly result in having two *neutrons* in the final state, while the absorption of π^+ mesons on a pair would predominantly result in final-state *proton* pairs. (The conventional model for pion absorption on a nucleon pair, which involves a rescattering on one nucleon before absorption on the other, can be called upon to support the above observation.) It follows that π^- absorption is enhanced over π^+ absorption because of the Coulomb-barrier penetration factors present in the wave functions of the final-state protons. These observations lead one to expect that the second-order potential will be more absorptive for π^- mesons, as is indicated by our phenomenological analysis. These observations may have interesting implications for the branching ratios $\sigma(\pi^+, pp)/\sigma(\pi^+, pn)$, $\sigma(\pi^-, nn)/\sigma(\pi^-, np)$, and $\sigma(\pi^+, pp)/\sigma(\pi^-, nn)$ for pions absorbed in flight. Of course, the connection between the cross sections for particular final states in pion induced reactions and the details of the optical potential which describes elastic scattering is not a simple matter in general.

The study of differences in the angular distributions of π^+ and π^- scattering cross sections has been suggested as a means to extract information about the neutron-matter radii of the Ca isotopes. However, as can be seen from Figs. 1–6, the second-order (ρ^2-dependent) potential is

quite important in the resonance region. Even at 241 MeV the first- and second-order cross sections are not quite the same. Since at pion energies above about 300 MeV the true pion absorption contribution to $V^{(2)}$ is expected to be much reduced, it may be useful to have data in that energy region. At high energies, however, other processes may make appreciable contributions to $V^{(2)}$. At this time, however, it does not appear possible to extract useful information concerning the neutron-matter distribution from the study of pion-nucleus scattering.

It is possible to define several scattering amplitudes, some of which are related to measurements of the total cross section for pion-nucleus scattering. The amplitude $F_N(\theta)$ is that which results upon neglecting the Coulomb interaction $\langle \vec{k}' | V_C | \vec{k} \rangle$. We note, however, that the strong interaction potential $\langle \vec{k}' | V^{(2)}(W) | \vec{k} \rangle$ is significantly different for π^+ and π^- mesons. [We recall that $\langle \vec{k}' | V^{(1)}(W) | \vec{k} \rangle$ also exhibits some differences for π^+ and π^- mesons; however, these differences are quite small.] The amplitude $F_N(0)$ is shown in Figs. 13(a) [$V^{(1)}$ only] and Fig. 13(b) [$V^{(1)} + V^{(2)}$]. The small difference in $F_N(0)$ for π^+ and π^- mesons exhibited in Fig. 13(b) reflects the above-mentioned isospin violation in $V^{(2)}$ (see Table II).

The nuclear amplitude which includes the effects of the Coulomb interaction,

$$f_N(0) = \frac{1}{2ik_0} \sum_{l=0}^{\infty} (2l+1) e^{2i\sigma_l} (\eta_l^c e^{2i\delta_l^c} - 1), \qquad (3.1)$$

is presented in Table II and in Fig. 13. Figure 13(c) exhibits the amplitude $f_N(0)$ calculated with $V^{(1)}$ only while Fig. 13(d) exhibits the result of a

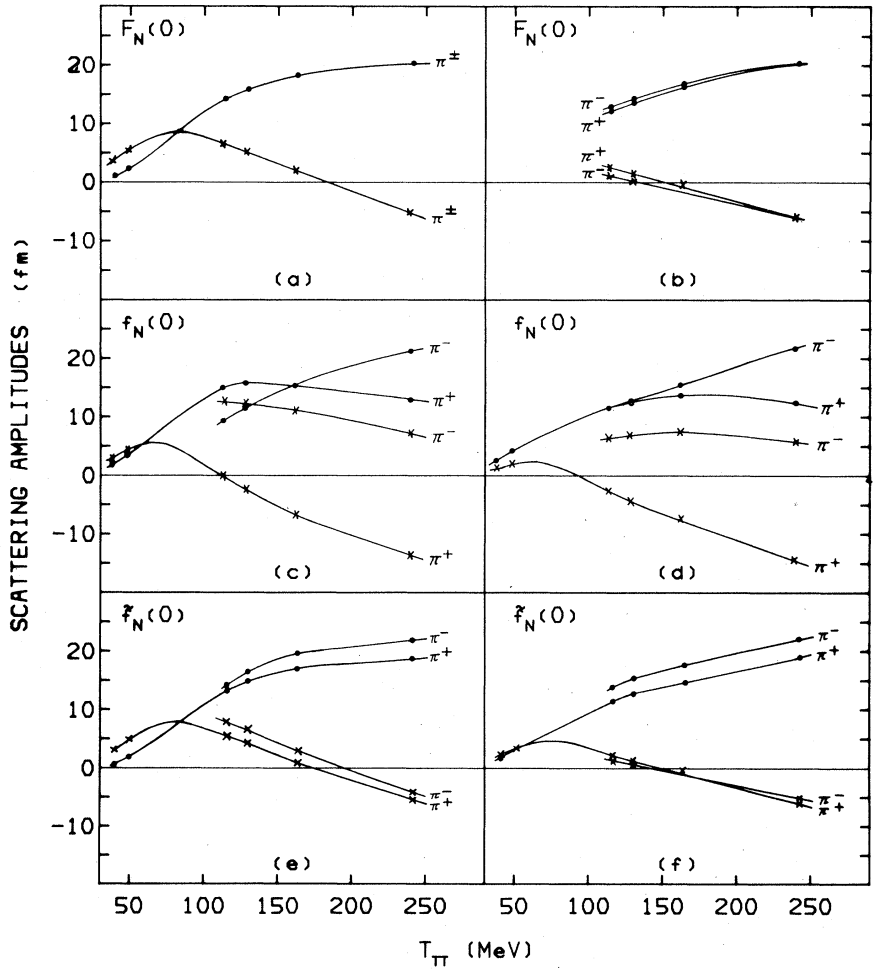

FIG. 13. Real (×) and imaginary (●) parts of the nuclear forward scattering amplitudes for ^{40}Ca vs incident π energy. (a), (c), and (e): with $V^{(1)}$; (b), (d), and (f): with $V^{(1)}+V^{(2)}$. Definitions of $F_N(0)$, $f_N(0)$, and $\tilde{f}_N(0)$ are given in the text. The curves are drawn only as a guide to the eye.

TABLE II. Calculated forward nuclear scattering amplitudes $f_N(0)$ and $\tilde{f}_N(0)$ (a) without and (b) with the second-order π-nucleus potential.

	T_π (MeV)	$f_N(0)$ (fm) (a)	(b)	$\tilde{f}_N(0)$ (fm) (a)	(b)
^{40}Ca, π^+	40	2.78 $+i1.81$	1.60 $+i2.74$	3.23 $+i0.776$	2.22 $+i1.74$
^{40}Ca, π^+	50	4.14 $+i3.38$	2.04 $+i4.27$	4.90 $+i1.98$	3.15 $+i3.02$
^{40}Ca, π^+	115.5	$-0.174+i15.0$	$-2.64+i11.7$	5.41 $+i13.3$	2.19 $+i11.4$
^{40}Ca, π^-	115.5	12.3 $+i9.33$	6.63 $+i11.5$	7.97 $+i14.3$	1.35 $+i13.8$
^{40}Ca, π^+	130	-2.29 $+i15.7$	$-4.15+i12.1$	4.17 $+i14.7$	1.22 $+i12.6$
^{40}Ca, π^-	130	12.2 $+i11.4$	6.91 $+i13.1$	6.67 $+i16.3$	0.629 $+i15.3$
^{40}Ca, π^+	163.5	-6.71 $+i15.9$	$-6.92+i13.3$	1.06 $+i16.9$	$-0.278+i15.0$
^{40}Ca, π^-	163.5	11.0 $+i15.3$	7.51 $+i15.5$	3.06 $+i19.4$	$-0.337+i17.6$
^{40}Ca, π^+	241	-13.5 $+i13.0$	-14.3 $+i12.4$	$-5.47+i18.4$	-6.45 $+i18.4$
^{40}Ca, π^-	241	7.17 $+i21.1$	6.05 $+i21.7$	$-4.26+i21.8$	-5.40 $+i21.6$
^{48}Ca, π^+	130	-1.99 $+i17.1$	$-3.23+i13.8$	5.09 $+i15.8$	2.83 $+i13.6$
^{48}Ca, π^-	130	13.7 $+i14.2$	11.9 $+i9.62$	6.34 $+i19.8$	6.61 $+i14.6$

calculation with $V^{(1)}+V^{(2)}$.

It is useful to define an additional amplitude,[13]

$$\tilde{f}_N(0)=\frac{1}{2ik_0}\sum_{l=0}^{\infty}(2l+1)(\eta_l^c e^{2i\delta_l^c}-1). \tag{3.2}$$

The amplitudes of Eqs. (3.1) and (3.2) may be used to define total cross sections[13]

$$\hat{\sigma}_{\rm tot}=\frac{4\pi}{k_0}\mathrm{Im}f_N(\theta=0) \tag{3.3}$$

and

$$\sigma_{\rm tot}=\frac{4\pi}{k_0}\mathrm{Im}\tilde{f}_N(\theta=0). \tag{3.4}$$

The relation of the cross sections defined in Eqs. (3.3) and (3.4) to experimental observations is discussed in Ref. 13. In this reference $\sigma_{\rm tot}$ [Eq. (3.4)] is denoted as σ_R and $\hat{\sigma}_{\rm tot}$ [Eq. (3.3)] is called σ_N. In Table III we present values for $\sigma_{\rm tot}$ [Eq. (3.4)], the elastic-scattering cross section $\sigma_{\rm el}$ and the reaction cross section σ_r calculated with and without the second-order potential. These quantities are exhibited in Fig. 14. In Fig. 14(a) (π^+) and Fig. 14(c) (π^-) we show the results of our calculations of the various cross sections including only the effects of $V^{(1)}$. Figures 14(b) (π^+) and 14(d) (π^-) are the results of a calculation including both $V^{(1)}$ and $V^{(2)}$.

IV. SUMMARY OF SALIENT FEATURES

We summarize some of our observations at this point:

(a) The first-order potential $V^{(1)}$ varies smoothly with energy with a maximum value for the matrix element $|\mathrm{Im}\langle\vec{k}|V^{(1)}|\vec{k}\rangle|$ at ~240 MeV.

TABLE III. Calculated cross sections (a) without and (b) with the second-order π-nucleus potential $\sigma_{\rm el}$: elastic scattering cross section $=\int|f_N|^2d\Omega=(\pi/k^2)\sum_{l=0}^{\infty}(2l+1)|\eta_l^c e^{2i\delta_l^c}-1|^2$, σ_r: reaction cross section $=(\pi/k^2)\sum_{l=0}^{\infty}(2l+1)[1-(\eta_l^c)^2]$, $\sigma_{\rm tot}$: total cross section $=\sigma_{\rm el}+\sigma_r=(4\pi/k)\times\mathrm{Im}\tilde{f}_N(\theta=0)$.

	T_π (MeV)	(a) $\sigma_{\rm el}$ (mb)	σ_r (mb)	$\sigma_{\rm tot}$ (mb)	(b) $\sigma_{\rm el}$ (mb)	σ_r (mb)	$\sigma_{\rm tot}$ (mb)
^{40}Ca, π^+	40	115.7	55.44	171.1	123.3	260.6	383.9
^{40}Ca, π^+	50	266.1	119.3	385.4	202.0	384.9	586.9
^{40}Ca, π^+	115.5	893.5	659.7	1553	526.1	812.4	1339
^{40}Ca, π^-	115.5	1028	646.1	1674	659.6	949.4	1609
^{40}Ca, π^+	130	844.3	750.2	1594	523.2	835.8	1359
^{40}Ca, π^-	130	1011	750.3	1761	690.5	966.5	1657
^{40}Ca, π^+	163.5	705.2	867.3	1572	540.5	852.3	1393
^{40}Ca, π^-	163.5	892.9	906.9	1800	697.6	941.8	1639
^{40}Ca, π^+	241	548.4	754.8	1303	588.1	714.4	1302
^{40}Ca, π^-	241	707.5	836.7	1544	742.2	788.1	1530
^{48}Ca, π^+	130	949.3	755.7	1705	615.2	852.0	1467
^{48}Ca, π^-	130	1239	902.2	2141	686.4	894.1	1580

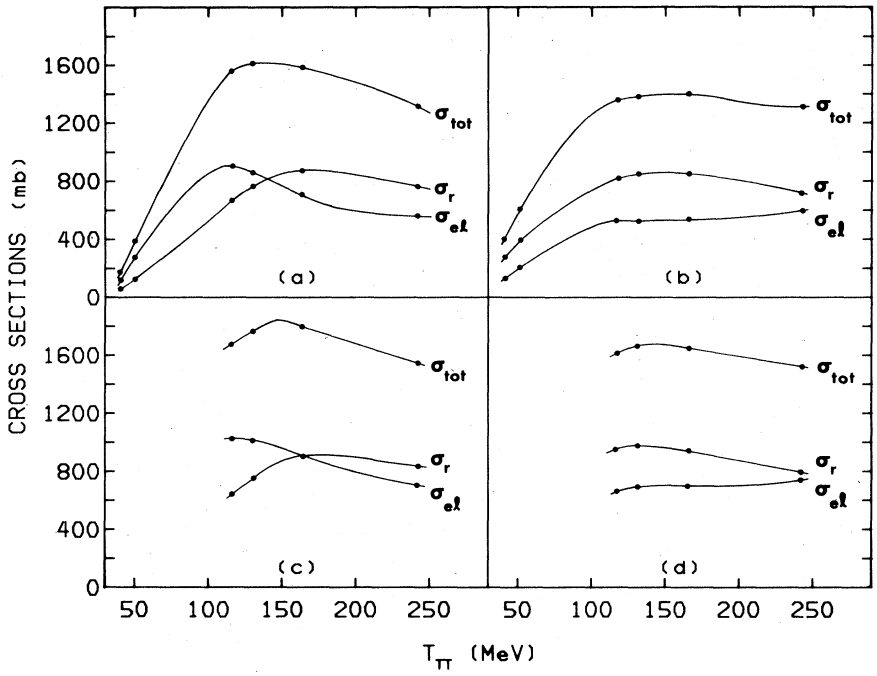

FIG. 14. Calculated total cross section (σ_{tot}), reaction cross section (σ_r), and elastic cross section (σ_{el}) vs pion energy. (a) $^{40}Ca(\pi^+)$ with $V^{(1)}$ only; (b) $^{40}Ca(\pi^+)$ with $V^{(1)}+V^{(2)}$; (c) $^{40}Ca(\pi^-)$ with $V^{(1)}$ only; (d) $^{40}Ca(\pi^-)$ with $V^{(1)}+V^{(2)}$. Curves are only drawn as a guide for the eye.

This maximum is at a greater energy than that which would be expected from the use of the fixed-scatterer approximation (FSA). The position of the maximum is determined in our calculation by nuclear binding and other off-shell effects[12] which are absent in FSA calculations.

(b) Inspection of Fig. 10 shows that the width at half maximum of $|\mathrm{Im}\langle\vec{k}|V^{(1)}|\vec{k}\rangle|$ is approximately 200 MeV for ^{16}O and ^{40}Ca. Again this is larger than the width that would be expected in the FSA and reflects the effects of a proper treatment of Fermi motion of the target particles. We remark that extraction of the spreading width Γ' of the Δ via an isobar-doorway calculation[11] of pion-nucleus scattering is made exceedingly difficult since simple kinematic considerations in the calculation of the first-order potential already provide a significant *apparent* broadening of the (3, 3) resonance.[14]

(c) The parameters of the second-order potential $V^{(2)}$ are determined phenomenologically and exhibit some notable features. The maximum of the value of $|\mathrm{Im}\langle\vec{k}|V^{(2)}|\vec{k}\rangle|$ appears at about 140–150 MeV for ^{16}O and ^{40}Ca (see Fig. 12). The value of the width at half maximum of this quantity is about 90 MeV. It is interesting to note that the cross section for the reaction $\pi+d\rightarrow p+p$ has a maximum value at approximately 140 MeV. The coincidence in energy of the maxima of the $\pi+d\rightarrow p+p$ cross section and the matrix element $|\mathrm{Im}\langle\vec{k}|V^{(2)}|\vec{k}\rangle|$ may provide some further support for the conjecture that $V^{(2)}$ describes, in the main, the effects of true pion absorption.[15]

(d) As may be seen from Fig. 12, the imaginary part of the second-order potential is significantly stronger for π^- scattering than for π^+ scattering at the same energy. An explanation for this behavior has been given in Sec. III. This explanation is consistent with our interpretation of the role of the second-order potential as describing the effects of true pion absorption.

V. CONCLUSIONS

Our studies of pion scattering from ^{12}C, ^{16}O, and ^{40}Ca have allowed us to discuss the systematic features of the pion-nucleus optical potential. This potential is composed of first- and second-order potentials which have different geometries. They also differ markedly in their energy dependence, which is a further indication that these potentials describe different physical processes. The analysis reported here should stimulate attempts to understand the second-order potential from a more fundamental point of view. Further, the development of a simple phenomenological form to represent the first-order potential should be facilitated. (A simple repre-

sentation of the entire optical potential would be useful for the rapid calculation of optical-model wave functions.)

We believe our analysis indicates the great importance of the proper treatment of off-shell effects and the effects of Fermi motion of the target nucleons. Before any investigation of true pion absorption effects or collision broadening is made, one finds a significant upward shift of the resonance position and a remarkable increase in the apparent width of the resonance due to the aforementioned effects.

ACKNOWLEDGMENT

This work was supported in part by the National Science Foundation and the PAC-BHE Faculty Award Program of the City University of New York. We wish to thank John Negele for providing us with a computer code for the calculation of Hartree-Fock wave functions.

[1]L. C. Liu, Phys. Rev. C 17, 1787 (1978); L. C. Liu and C. M. Shakin, *ibid.* 19, 129 (1979).

[2]L. Celenza, L. C. Liu, and C. M. Shakin, Phys. Rev. C 11, 1593 (1975); 12, 721(E) (1975).

[3]Calculations which are similar to ours are reported in J. P. Maillet, J. P. Dedonder, and C. Schmitt, Nucl. Phys. A316, 267 (1979).

[4]E. Friedman, H. J. Gils, H. Rebel, and Z. Majka, Phys. Rev. Lett. 41, 1220 (1978) and references therein.

[5]A. Chaumeaux, V. Layly, and R. Schaeffer, Phys. Lett. 72B, 33 (1977) and references therein.

[6]M. J. Jakobson, G. R. Burleson, J. R. Calarco, M. D. Cooper, D. C. Hagerman, I. Halpern, R. H. Jeppeson, K. F. Johnson, L. D. Knutson, R. E. Marrs, H. O. Meyer, and R. P. Redwine, Phys. Rev. Lett. 38, 1201 (1977).

[7]Similar phenomenological forms are used in the momentum-space calculations of R. H. Landau and A. W. Thomas, Nucl. Phys. A302, 461 (1978). For a review of the most recent coordinate-space calculations of the Michigan State University group see, H. McManus, Invited talk at Second International Conference on Meson-Nuclear Physics, Houston, Texas, 1979 (unpublished).

[8]Q. Ingram, E. Boschitz, L. Pflug, J. Zichy, J. P. Albanèse, and J. Arvieux, Phys. Lett. 76B, 173 (1978).

[9]J. P. Egger, R. Corfu, P. Gretillat, C. Lunke, J. Piffaretti, E. Schwarz, C. Perrin, J. Jansen, and B. M. Preedom, Phys. Rev. Lett. 39, 1608 (1977); B. M. Preedom, in *Proceedings of the Seventh International Conference on High-Energy Physics and Nuclear Structure, Zurich, 1977,* edited by M. P. Locher (Birkhauser, Basel, 1977), p. 119.

[10]C. M. Ko and D. O. Riska, Nucl. Phys. A312, 217 (1978); J. Chai and D. O. Riska, Phys. Rev. C 19, 1425 (1979); G. F. Bertsch and D. O. Riska, Phys. Rev. C 18, 317 (1978) and references therein. See also, F. Hachenberg, H. J. Pirner, and J. Hüfner, Phys. Lett. 66B, 425 (1977).

[11]F. Lenz, Ann. Phys. (N.Y.) 95, 348 (1975); M. Hirata, F. Lenz, and K. Yazaki, *ibid.* 108, 16 (1977); M. Hirata, J. H. Koch, F. Lenz, and E. J. Moniz, Phys. Lett. 70B, 281 (1977); W. Weise, Nucl. Phys. A278, 402 (1977); E. Oset and W. Weise, Phys. Lett. 77B, 159 (1978); E. Oset and W. Weise, Nucl. Phys. A319, 477 (1979); K. Klingenbeck, M. Dillig, and M. G. Huber, Phys. Rev. Lett. 41, 387 (1978); M. G. Huber and K. Klingenbeck, Lectures at the Massurian Summer School, Mikolajki, 1978 (unpublished); G. E. Brown and W. Weise, Phys. Rep. 22C, 280 (1975).

[12]Other authors use different prescriptions in the specification of the energy which appears in the pion-nucleon T matrix. For example, see Refs. 3 and 7.

[13]M. D. Cooper and M. B. Johnson, Nucl. Phys. A260, 352 (1976).

[14]A careful treatment of this effect appears in the work of Oset and Weise (Ref. 11); however, this kinematic broadening of the resonance is not discussed in their published work.

[15]We refer the reader to Ref. 7 for a recent discussion of TPA and the quasideuteron model.